PCCP

ARTICLE

A theoretical and shock tube kinetic study on hydrogen abstraction from phenyl formate†

Received 00th January 20xx,
Accepted 00th January 20xx

DOI: 10.1039/x0xx00000x

www.rsc.org/

Hongbo Ning, [ab] Dapeng Liu, [c] Junjun Wu, [ab] Liuhao Ma, [ab] Wei Ren *[ab] and Aamir Farooq [c]

Hydrogen abstraction reactions of phenyl formate (PF) by different radicals (H/O(^{3}P)/OH/HO_2) were theoretically investigated. We calculated the reaction energetics for PF + H/O/OH using the composite method ROCBS-QB3//M06-2X/cc-pVTZ and that for PF + HO_2 at the M06-2X/cc-pVTZ level of theory. The high-pressure limit rate constants were calculated using the transition state theory in conjunction with the 1-D hindered rotor approximation and tunneling correction. Arrhenius expressions of rate constants were provided over the temperature range of 500–2000 K. To validate the theoretical calculations, the overall rate constants of PF + OH → Products were measured in shock tube experiments at 968–1128 K and 1.16–1.25 atm using OH laser absorption. The predicted overall rate constants agree well with the shock tube data (within 15%) over the entire experimental conditions. Rate constant analysis indicates that the H-abstraction at the formic acid site dominates the PF consumption, whereas the contribution of H-abstractions at the aromatic ring increases with temperature. Additionally, comparisons of site-specific H-abstractions from PF with methyl formate, ethyl formate, benzene, and toluene were performed to understand the effects of the aromatic ring and side-chain substituent on H-abstraction rate constants.

1. Introduction

Biodiesels produced from vegetable oils, animal fats and microalgae have drawn increasing attention and were recently used in blends with Jet A for aircraft engines at cruise conditions.[1] The presence of ester moiety in biodiesel components makes different combustion properties from conventional fossil fuels.[2] Most of the recent theoretical and experimental studies focused on small alkyl esters. Peukert et al.[3] explored the thermal decomposition of methyl formate (MF) and methyl acetate (MA) using the CCSD(T)/CBS//B3LYP/6-311++G(d,p) method. Tan et al.[4–6] systematically studied the H-abstraction reactions of C_2–C_4 methyl esters using CCSD(T)/CBS and MRSDCI methods. The Stanford group performed series of experimental studies of C_2–C_5 methyl and ethyl esters using shock tube and laser absorption measurements.[7–10] Very recently, Sun et al.[11] conducted systematical studies of combustion kinetics of C_3–C_5 ethyl esters using experiment and theory; time-of-flight mass spectrometry (TOFMS) and CCSD(T)/CBS//M06-2X/cc-pVTZ method.

In this work, we extended the chemical kinetics studies from straight-chain alkyl esters to aromatic esters to further examine the kinetic effects of aromatic ring on ester group. Phenyl formate (PF) is the simplest aromatic ester which can be formed by esterification of phenol with formic acid. Additionally, thermal decomposition of PF molecules directly produces many important combustion intermediates, *i.e.*, HCO, HCOO, and C_6H_5, making it a potential candidate or precursor for chemical kinetics studies of these radicals. Under typical combustion conditions, H-abstraction reaction is of critical importance to fuel consumption and intermediate species formation. Moreover, the importance of H-abstractions by different radicals varies with temperatures, *i.e.*, approximately, H-abstraction by OH plays an important role at > 500 K; by HO_2 at 800−1300 K; and by O(^{3}P), H and CH_3 at > 1300 K. Hence, this work aims to provide a complete study on the rate constants for H-abstractions of PF by H/O(^{3}P)/OH/HO_2 radicals using *ab initio*/statistical rate theory.

Briefly, we first calculated the bond dissociation energies (BDEs) of all the C–O and C–H bonds in PF using the ROCBS/QB3//M06-2X/cc-pVTZ method. Then the H-abstraction rate constants by H/O/OH/HO_2 radicals were determined using the canonical transition state theory in conjunction with the hindered rotor approximation and tunneling correction. The overall rate constants of PF + OH were also measured in shock tube experiments to validate the current theoretical results.

2. Computational details

Molecular structures and vibrational frequencies were calculated at the M06-2X/cc-pVTZ level[12] using the Gaussian 09 package.[13] The obtained frequency and zero-point energy (ZPE) values were scaled by 0.985 and 0.971, respectively, to account

[a] Department of Mechanical and Automation Engineering, The Chinese University of Hong Kong, New Territories, Hong Kong.
[b] Shenzhen Research Institute, The Chinese University of Hong Kong, New Territories, Hong Kong.
[c] King Abdullah University of Science and Technology, Clean Combustion Research Center, Physical Sciences and Engineering Division, Thuwal 23955, Saudi Arabia.
†Electronic Supplementary Information (ESI) available. See
DOI: 10.1039/x0xx00000x

for the anharmonicity.[12] Each transition state (TS) was confirmed by one single imaginary vibrational frequency and the intrinsic reaction coordinate (IRC) analysis to ensure its connection with the desired reactants and products. A barrierless entrance channel exists for H-abstractions by OH and HO_2, leading to the van der Waals complexes (*i.e.*, reactant complex, RC; product complex, PC) that can be captured by further optimizing the reactant and product ends of the IRC analysis. Due to the heavy spin contamination caused by the delocalized aromatic ring, the accurate electronic energies were calculated at the ROCBS-QB3 level,[14] which uses spin-restricted wave functions to eliminate the empirical correction for the spin contamination in CBS-QB3. This strategy was previously applied for studying other similar reactions such as *m*-xylene + OH.[15] For the low-frequency torsional modes, the relaxed PES scans of reactants, TSs and products were carried out (10° increment) as a function of the corresponding dihedral angle at the M06-2X/6-31G(d,p) level. The obtained potential was then used to determine the lowest energy conformer and the hindered rotor correction for rate constant calculations.

Based on the calculated energies and molecular properties, all the high-pressure limit rate constants for H-abstraction reactions were calculated using transition state theory (TST) with the tunneling correction and 1-D hindered rotor correction in the KiSThelP platform.[16] The rate constant is described by the following equation:

$$k^{\mathrm{TST}}(T) = \chi(T) \cdot \sigma \frac{k_b T}{h} \frac{Q^{\mathrm{TS}}(T)}{Q^{\mathrm{R}}(T)} exp\left(-\frac{V^{++}}{k_b T}\right), \quad (1)$$

where $\chi(T)$ is the Eckart tunneling correction coefficient,[17] V^{++} is the activation energy of the considered reaction including ZPEs, σ is the reaction path degeneracy, k_b is the Boltzmann constant, h is the Planck constant, T is temperature, $Q^{TS}(T)$ and $Q^{R}(T)$ are the partition functions of TSs and reactants, respectively. Finally, the rate constants are fitted to the modified three-parameter Arrhenius expression that is commonly adopted in a reaction mechanism.

Uncertainties of the theoretically determined rate constants are mainly from three aspects. Firstly, the predicted energy using the ROCBS-QB3 method has an uncertainty of ~1.2 kcal mol^{-1}, which is estimated from the mean absolute deviation of a set of open-shell radicals.[14] Its contribution to the rate constant uncertainty is evaluated to be 1.8 times at 1000 K and 1.35 times at 2000 K. Secondly, the frequency scaling factor is considered another factor that affects the calculation accuracy. Xing et al.[18] previously used the global uncertainty analysis for studying ethanol decomposition and obtained an uncertainty factor of 25–30% for the rate constant determination. Thirdly, the hindered rotors caused by H-bond interactions tend to be more prevalent among molecules or complexes with multiple oxygenated moieties, which lead to the coupling of internal rotors. Sharma et al.[19] and Tao et al.[20] used the 1-D hindered rotor model to predict the kinetic and thermodynamic properties of ROO and HOOQOOH, as well as reactions of the methyl octanoate peroxy radical. Hence, we believe that the 1-D hindered rotor model can be used for calculating the rate constants for H-abstractions of PF as a compromise between computational accuracy and complexity. Jasper et al.[21] have discussed in detail the uncertainty contributions of barrier height, partition function and tunneling effect to the rate constants for the H-abstractions of fulvene, which is similar to our reaction system. We have calculated the overall uncertainty of the rate constant and obtained a factor of <3 between 1000 K and 2000 K.

3. Shock tube/laser absorption experiment

Rate constant measurements of PF with hydroxyl radical (PF + OH → Products) were carried out behind reflected shock waves in the low-pressure shock tube at King Abdullah University of Science and Technology (KAUST). The progress of the reaction was followed by monitoring the OH concentration. Hydroxyl radicals were detected at the $R_1(5)$ rovibrational transition of the A–X (0,0) band near 306.7 nm using a narrow-linewidth (< 200 kHz) continuous wave UV laser. Details about the shock tube and laser system can be found elsewhere;[22] only the brief description is given here. Laser absorption diagnostics for the other radicals such as H, O and HO_2 are currently not available

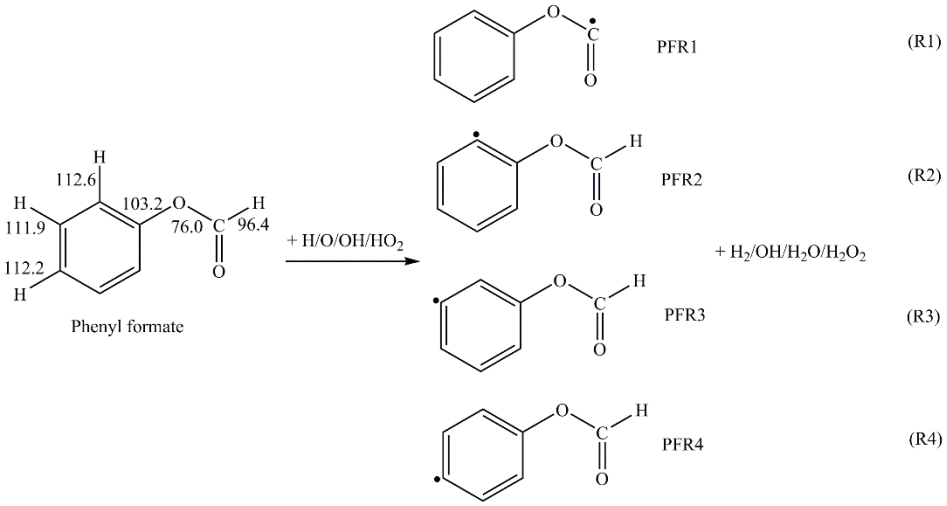

Fig. 1 BDEs (kcal mol^{-1}) of PF calculated at the ROCBS-QB3//M06-2X/cc-pVTZ level and H-abstraction reaction pathways.

for shock tube experiments. Here, we only report the measured rate constants of PF with hydroxyl radical.

The shock tube is composed of a 9 m long driven section and 9 m long driver section. The driver section is modularized and the length can be adjusted according to the test time requirement. The diameter of the shock tube is 14.2 cm. The shock tube driven section is evacuated before each experiment with a turbo molecular pump to a pressure of about 1×10^{-5} Torr to eliminate impurities. *Tert*-butyl hydroperoxide (TBHP) was used as a thermal precursor for OH radicals in this study since it decomposes very rapidly (less than 10 μs at $T > 800$ K; less than 1 μs at $T > 1100$ K) to produce OH and other less reactive radicals. A mixture of 300 ppm PF and 18 ppm TBHP in argon was prepared in a mixing vessel equipped with a turbo molecular vacuum pump and a magnet mixing stirrer. The mixture was left to homogenize for at least 2 hours prior to experiments. The TBHP aqueous solution (70% TBHP/30% H_2O) and PF (>98% purity) were obtained from Sigma-Aldrich. Incident shock velocity measurements were carried out using five PZT pressure transducers (PCB 113B26) placed over the last 1.5 m of the driven section of the shock tube. The pre-shock pressure (P_1) in the driven section was measured using two high-accuracy Baratron pressure transducers. Temperatures and pressures behind reflected shock waves (T_5 and P_5) were determined using the standard shock-jump relations with the measured incident shock speed and known thermodynamic parameters as the inputs.

The UV beam (~20 mW) was generated by frequency doubling the red beam near 613.4 nm (~1 W) generated by a cw ring-dye laser that was pumped by a Nd:YAG laser at 532 nm (~10 W). To minimize the noise caused by laser intensity fluctuations, a common-mode-rejection scheme was applied by splitting the UV beam with a beam splitter prior to the shock tube. Beer-Lambert law, $I/I_0 = \exp(-k_{OH}X_{OH}PL)$, was used to convert the measured signal to absolute OH concentration, where I and I_0 are the transmitted and incident laser intensities, k_{OH} is the OH absorption coefficient, X_{OH} is the OH mole fraction, P is the total pressure (atm), and L is the absorption path length (14.2 cm). The estimated uncertainty in the measured OH mole fraction (X_{OH}) is approximately ±3%, mainly due to the uncertainties in the reflected-shock temperature and hydroxyl absorption coefficient.[23] The minimum detectable hydroxyl mole fraction is less than 1 ppm.

4. Results and discussion

The PF conformer with the lowest energy was determined by scanning the PES for all the internal rotational degrees of freedom and subsequently selecting the global minimum point for the further optimization. Fig. 1 depicts four H-abstraction channels of PF to form PFR1–PFR4 radicals. Note that it is hard for PF to produce CH_3 via the direct bond fission, and we only consider the H-abstractions by the other four radicals including H, O, OH and HO_2. The PF + H/O and PF + OH/HO_2 reactions are discussed in sections 4.1 and 4.2, respectively, as the latter reactions involve the H-bond with extra complications.

The calculated BDEs of PF are also shown in Fig. 1; the detailed structural information is given in the ESI†. Comparing the two C–O bonds, it is interesting to observe that the HC(=O)–OC_6H_5 bond (76.0 kcal mol^{-1}) has a much smaller BDE than the HC(=O)O–C_6H_5 bond (103.2 kcal mol^{-1}). It is known that the BDE of the RC(=O)–OCH_3 bond (~100.0 kcal mol^{-1}) in the alkyl ester (*i.e.*, MF, MA, MP and MB) is larger than that of RC(=O)O–CH_3 (~86.0 kcal mol^{-1}).[24] Such a difference is possibly caused by the delocalized π-bond π_7^8 formed by the lone pair of O-atom in the ester group of PF with the six carbons in the aromatic ring. This π-bond makes the electronic density of O-atom shift toward the aromatic ring and thus weakens the HC(=O)–OC_6H_5 bond. Among all the C–H bonds, the BDE calculation suggests that the H atom at the formic acid site is the easiest to be abstracted, followed by the H atoms at *m*-site, *o*-site and *p*-site, respectively.

4.1 PF + H/O reactions

Considering the kinetic similarity of PF + H/O, only the structures and energies for PF + H are discussed here. Regarding the TS formation in PF + H reactions, the breaking C–H bonds are elongated by ~0.3 Å, and the angles between the breaking and forming bonds are ~180°. Table 1 lists the ZPE-corrected energies of TSs (barrier heights) and products relative to reactants at the ROCBS-QB3//M06-2X/cc-pVTZ level. The barrier heights of the four reaction channels, *i.e.*, E(TS1) < E(TS3) < E(TS2) ~ E(TS4), exhibit the same trend as BDEs. The detailed relative energies of PF + O are provided in Table S1 of ESI†. Note that the barrier heights of PF + O are consistently lower than

Table 1 Relative energies (kcal mol^{-1}) for reactions PF + H and PF + OH at the ROCBS-QB3//M06-2X/cc-pVTZ level of theory (at 0 K including zero-point energies).

Reactants	RCs	TSs	PCs	Products
PF + H (0.0)	-	9.2	-	PFR1 + H_2 (-8.0)
PF + H (0.0)	-	15.8	-	PFR2 + H_2 (8.3)
PF + H (0.0)	-	14.7	-	PFR3 + H_2 (7.6)
PF + H (0.0)	-	15.2	-	PFR4 + H_2 (7.9)
PF + OH (0.0)	-1.5	0.9	-22.5	PFR1 + H_2O (-21.2)
PF + OH (0.0)	-1.5	4.1	-4.6	PFR2 + H_2O (-4.9)
PF + OH (0.0)	-2.1	4.0	-6.4	PFR3 + H_2O (-5.6)
PF + OH (0.0)	-5.4	4.0	-5.4	PFR4 + H_2O (-5.3)

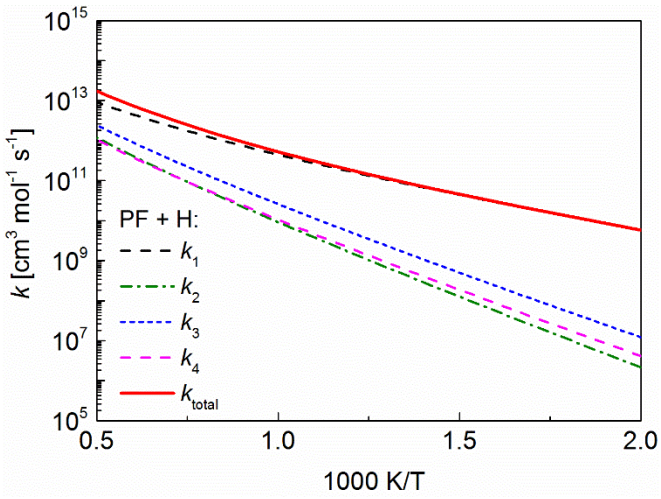

Fig. 2 Rate constants for PF + H reactions determined in this work.

that of PF + H reactions by ~5 kcal mol^{-1} in terms of H-abstractions from the aromatic ring.

The high-pressure limit rate constants for PF + H/O were calculated at 500–2000 K using the TST with 1-D hindered rotor approximation; the Arrhenius expressions are given in Table S2 of ESI†. Note that the Eckart tunneling correction is not applicable for certain reaction channels with negative energy barriers (see Table S1). Thus, the Winger method[25] was used instead to account for the tunneling effect as the deviation between the Eckart and Winger corrections is only 6–20% over the temperature range of 500–2500 K.[26] As no relevant experimental and theoretical results were reported in the literature, Fig. 2 only presents the rate constants for PF + H determined in this work. Among all the reaction channels, R1 dominates the entire temperature range, which is consistent with the previous energy barrier analysis (R1 channel is ~ 6 kcal mol^{-1} lower than R2–R4). In comparison, for the PF + O reactions shown in Fig. S1 of ESI†, R1 channel has the largest rate constant but R3/R4 also play important roles particularly at higher temperatures. The energy barriers for R1–R4 reactions of PF + O are 8.3, 10.9, 9.9 and 10.2 kcal mol^{-1}, respectively.

4.2 PF + OH/HO_2 reactions

H-abstractions of PF by OH and HO_2 radicals proceed via more complex reaction pathways. RCs and PCs are possibly formed via H-bonds between PF and the abstracting radicals or products. Fig. 3 depicts the TS structures for PF + OH/HO_2 reactions. For PF + OH reactions, the OH group of TS1 is located above the aromatic ring to form the H–O–H–C plane that is nearly perpendicular to the benzene ring. TS2 is stabilized by two H-bonds (2.595 and 2.524 Å) to form two six-member rings. TS3 and TS4 have one H-bond (2.546 and 2.538 Å) and the OH radical is perpendicular to the benzene ring plane. Compared with the TSs of other methyl esters (MF,[4] MA,[5] MP[6] and EF[26]) that have H-bond lengths of 1.970–2.220 Å, the influence of H-bond on the energies of PF is not as obvious as the alkyl esters due to the longer H-bond. For the PF + HO_2 reactions, all the four TSs are stabilized by the H-bond formed between the carbonyl oxygen and H-atom in the benzene ring. Additionally, TS3 and TS4 have another H-bond formed between the H-atom in the benzene ring and the O-atom of HO_2.

In general, PF + OH/HO_2 reactions proceed via a three-step process: PF + OH/HO_2 ↔ RCs → PCs ↔ Products. For PF + OH reactions, it is seen in Table 1 that the energy barriers of PCs ↔ Products are 0.1–1.3 kcal mol^{-1}, which are dramatically lower than that of PCs → RCs (8.7–23.4 kcal mol^{-1}). Therefore, the contribution of PCs to the overall H-abstraction rate constants is negligible. In contrast, the energy barriers of RCs ↔ PF + OH are 1.5–5.4 kcal mol^{-1}, which are comparable to that of RCs → PCs (2.4–9.4 kcal mol^{-1}). Thus, RCs should be considered when calculating the overall H-abstraction rate constants. It is noteworthy that the PF + HO_2 reactions have energy barriers of 16.5–24.5 kcal mol^{-1} (see Table S1), higher than that for PF + H/O/OH. The higher energy barriers of HO_2 abstractions suggest a minor contribution of RCs and PCs to the overall rate constants.[5,6] However, it should be pointed out that the relative energies of TSs for PF + HO_2 cannot be obtained at the ROCBS-QB3 level due to the limited computing capability. Hence, the energy barriers and rate constants for PF + HO_2 were calculated at the M06-2X/cc-pVTZ level instead.

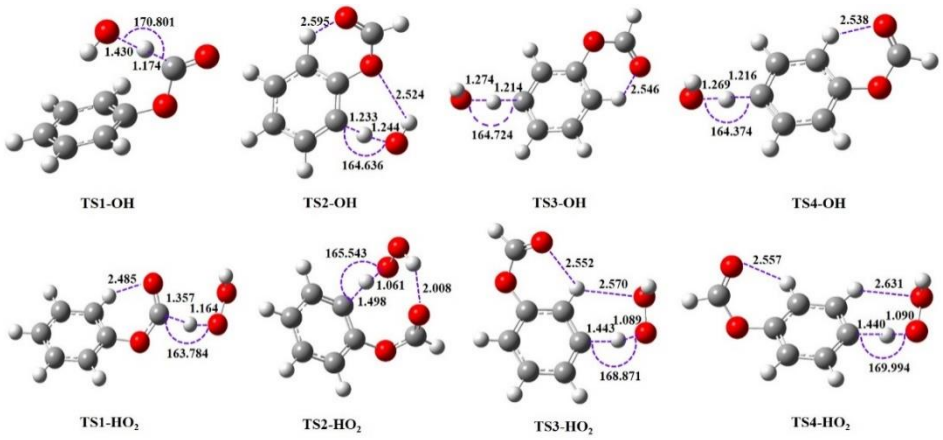

Fig. 3 Optimized geometries (angstroms and degrees) of TSs for PF + OH/HO_2 reactions at the M06-2X/cc-pVTZ level of theory.

PCCP

ARTICLE

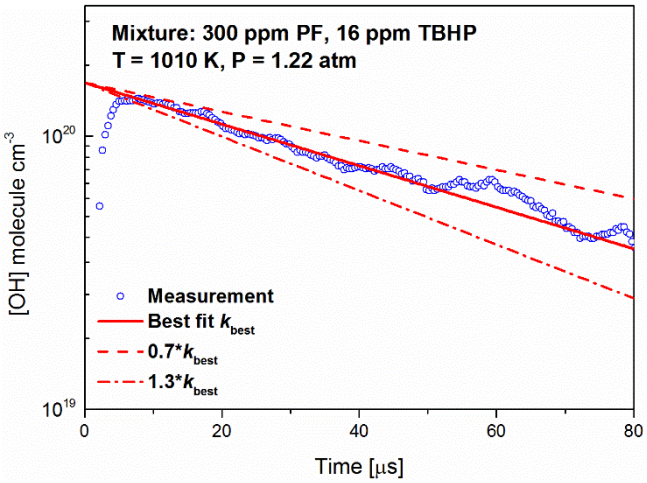

Fig. 4 Measured OH concentration (molecule cm^{-3}); the best fit and perturbations of ±30% are also plotted.

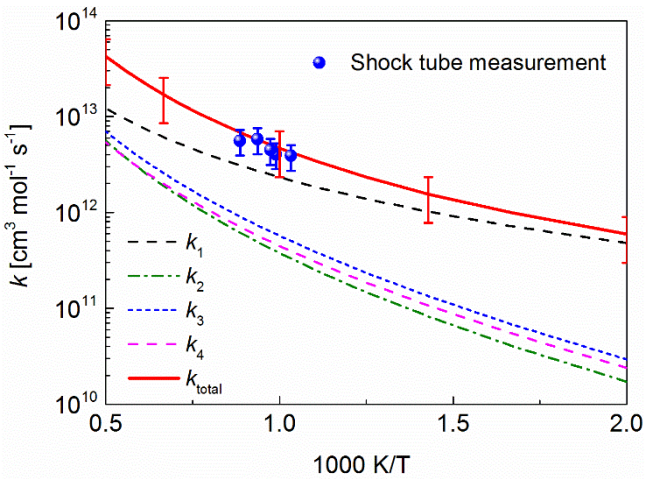

Fig. 5 Calculated site-specific H-abstraction rate constants, overall rate constants and shock tube experimental data (symbol) for PF + OH → Products.

Table 2 Measured rate constants for PF + OH → Products.

T_5 (K)	P_5 (atm)	k (cm^3 $molecule^{-1}$ s^{-1})
968	1.25	6.45 x 10^{-12}
1010	1.22	6.7 x 10^{-12}
1027	1.25	7.43 x 10^{-12}
1067	1.16	9.63 x 10^{-12}
1128	1.18	9.29 x 10^{-12}

The rate constants for these reaction schemes are normally calculated using two strategies such as the canonical TST and the two-TS model including VRC-TST. Previous studies[5,6] adopted the two-TS model to identify the outer TSs which only matter at very low temperatures (< 200 K). The inner TSs are rate-limiting over the temperature range of 500–2000 K. Additionally, the H-bonds of RCs are rather unstable at higher temperatures. Hence, it is fairly justified to use TST to calculate the rate constants for PF + OH/HO_2 in this study. It is also kinetically robust to ignore the RC formation for rate constant calculations. Table S2 in ESI† lists the parameters of the fitted Arrhenius expressions for PF + OH/HO_2.

The calculated rate constants for PF + OH → Products are compared with the shock tube measurements conducted at 968–1128 K and 1.16–1.25 atm. Fig. 4 presents one representative hydroxyl concentration profile measured using the UV laser absorption. The rate constant is extracted as $k_{PF+OH} = k_{1st}/[PF]_0$, where k_{1st} is the slope of ln([OH]) plot in Fig. 4 and $[PF]_0$ is the initial concentration of phenyl formate. The k_{1st} is calculated to be 4416.4 s^{-1} for the representative case shown in Fig. 4, which gives a second order rate of 6.7×10^{-12} cm^3 $molecule^{-1}$ s^{-1}. Uncertainty in the rate constant measurement is estimated to be ±20 % which primarily comes from uncertainties in mixture composition, temperature, pressure and fitting method. Table 2 summarizes the experimentally determined rate constants at 968–1128 K.

Fig. 5 presents the computed site-specific H-abstraction rate constants (k_1–k_4), the overall rate constants (k_{total}) and the shock tube measurements. Our calculations of the overall rate constants agree well with the shock tube data with a deviation of 15% over the experimental temperature range. The good agreement validates the rational of using TST to calculate the rate constants at high temperatures. It is also noteworthy that the H-bonds indeed lower the relative energy of a molecular structure and its entropy as well. However, the relative energy and entropy have opposite influences on rate constants and temperature dependences. The decreased entropy may compensate (or exceed) the influence of energy reduction on rate constants.[27] Hence, although R2–R4 have almost the same energy barriers, the rate constant of R2 is smaller than the other two reactions mostly due to the lower entropy of TS2. The similar behavior is observed for reaction R2 of PF + HO_2 shown in Fig. S1 of ESI†. The transition state TS2 has the lowest energy barrier but the smallest rate constant, which is mainly due to the influence of entropy.

Finally, based on the results obtained in this work and the previous studies, we are able to investigate the effects of the aromatic ring and side-chain substituent on H-abstraction rate constants. Fig. 6 compares the rate constants for H-abstractions

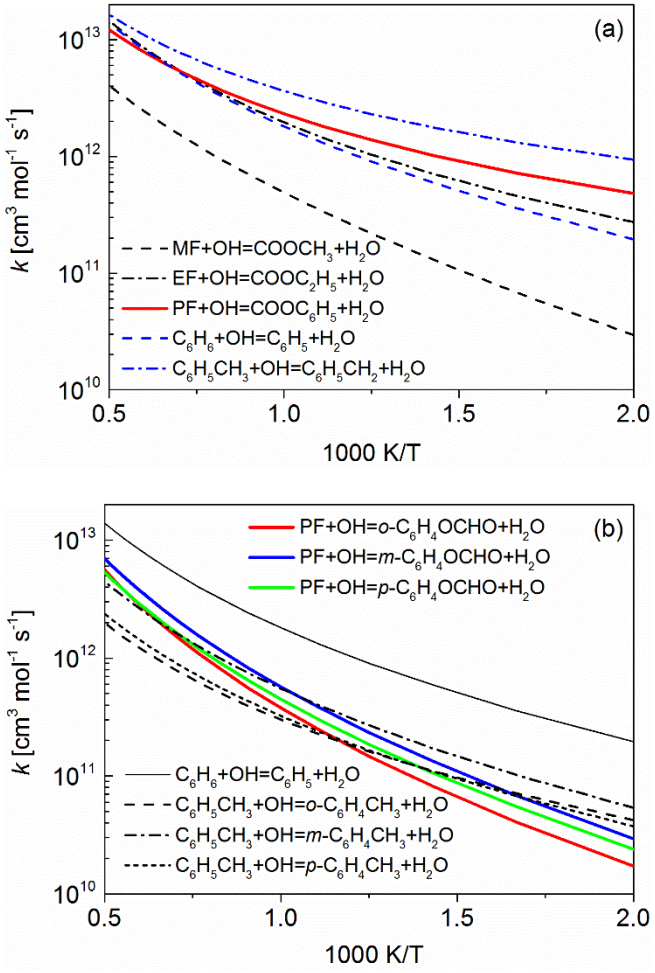

Fig. 6 Comparison of the H-abstraction rate constants for MF,[4] EF,[26] C_6H_6,[28] $C_6H_5CH_3$[28] and PF (this work) by OH.

from MF,[4] ethyl formate (EF),[26] benzene,[28] toluene[28] and PF by OH. Comparing the H-abstraction at the carbonyl site from MF, EF and PF, reaction (PF + OH) has the largest rate constant, followed by reactions (EF + OH) and (MF + OH) shown in Fig. 6(a). Comparing H-abstractions at the side chain of the aromatic ring (toluene and PF), reaction ($C_6H_5CH_3$ + OH) has the largest rate constant, followed by reactions (PF + OH) and (C6H6 + OH). It is qualitatively speculated that the aromatic ring of PF promotes the H-abstraction at the carbonyl site compared with the straight substituents (CH_3 in MF, C_2H_5 in EF). Moreover, the H-atom in the side chain is abstracted more easily than the aromatic ring. Fig. 6(b) also examines the influence of the existence of a substituent when abstracting hydrogen from the aromatic ring. Compared with benzene, the presence of a substituent (CH_3 in toluene and HCOO in PF) significantly inhibits the H-abstraction from the aromatic ring.

Conclusions

H-abstraction reactions of PF by H/O/OH/HO_2 radicals were theoretically investigated in this work. Rate constants were calculated using the TST coupled with 1-D hindered rotor approximation and tunneling correction at 500–2000 K. The rate constants for PF + OH were also measured in the shock tube using UV absorption of OH over the temperature range of 968–1128 K and pressures around 1 atm. Our calculations agree well with the experimental data (within 15%). Rate constant analysis indicates that the H-abstraction from the formic acid site dominates the consumption of PF. The detailed comparison of the H-abstraction rate constants for MF, EF, benzene, toluene and PF indicates that the presence of the aromatic ring in formate esters makes it behave differently from alkyl esters regarding the reactivity and molecular property. We believe that the computed H-abstraction rate constants for PF can be used for the detailed combustion modeling of PF and other aromatic esters.

Conflicts of interest

There are no conflicts to declare.

Acknowledgements

This work is supported by National Natural Science Foundation of China (51776179) and Research Grants Council of the Hong Kong SAR, China (14234116). Shock tube experiments were carried out at KAUST and this work was funded by Competitive Center Funding (CCF) program at KAUST. We are also thankful to Shenzhen Supercomputing Center for providing computational facilities.

References

1 R.H. Moore, K. L. Thornhill and B. Weinzierl, et al., *Nature*, 2017, **543**, 411–415.
2 P. Diévart, S.H. Won, S. Dooley, F.L. Dryer and Y. Ju, *Combust. Flame*, 2012, **159**, 1793–1805.
3 S.L. Peukert, R. Sivaramakrishnan, M.-C. Su and J.V. Michael, *Combust. Flame*, 2012, **159**, 2312–2323.
4 T. Tan, M. Pavone, D.B. Krisiloff and E.A. Carter, *J. Phys. Chem. A*, 2012, **116**, 8431–8443.
5 T. Tan, X. Yang, C.M. Krauter, Y. Ju and E.A. Carter, *J. Phys. Chem. A*, 2015, **119**, 6377–6390.
6 T. Tan, X. Yang, Y. Ju and E.A. Carter, *Phys. Chem. Chem. Phys.*, 2016, **18**, 4594–4607.
7 K.-Y. Lam, D.F. Davidson and R.K. Hanson, *J. Phys. Chem. A*, 2012, **116**, 12229–12241.
8 A. Farooq, D.F. Davidson, R.K. Hanson and C.K. Westbrook, *Fuel*, 2014, **134**, 26–38.
9 W. Ren, E. Dames, D. Hyland, D.F. Davidson and R.K. Hanson, *Combust. Flame*, 2013, **160**, 2669–2679.
10 W. Ren, R. Mitchell Spearrin, D.F. Davidson and R.K. Hanson, *J. Phys. Chem. A*, 2014, **118**, 1785–1798.
11 W. Sun, T. Tao, R. Zhang, H. Liao, C. Huang, F. Zhang, X. Zhang, Y. Zhang and B. Yang, *Combust. Flame*, 2017, **185**, 173–187.
12 Y. Zhao and D.G. Truhlar, *Theor. Chem. Acc.*, 2008, **120**, 215–241.
13 M.J. Frisch, G.W. Trucks and H.B. Schlegel, et al., Gaussian 09, revision D.01, Gaussian, Inc., Wallingford, CT, 2009.
14 G.P.F. Wood, L. Radom, G.A. Petersson, E.C. Barnes, M.J. Frisch and J.A. Montgomery Jr., *J. Chem. Phys.*, 2006, **125**, 094106–094120.
15 S.S Pan and L.M. Wang, *J. Phys. Chem. A*, 2014, **118**, 10778–10787.

16 S. Canneaux, F. Bohr and E. Henon, *J. Comput. Chem.*, 2014, **35**, 82–93.
17 C. Eckart, *Phys. Rev.*, 1930, **35**, 1303−1309.
18 L. Xing, S. Li, Z. Wang, B. Yang, S.J. Klippenstein and F. Zhang, *Combust. Flame*, 2015, **162**, 3427–3436.
19 S. Sharma, S. Raman and W.H. Green, *J. Phys. Chem. A*, 2010, **114**, 5689–5701.
20 H.R. Tao and K.C. Lin, *Combust. Flame*, 2017, **180**, 148−157.
21 A. W. Jasper and N. Hansen, *Proc. Combust. Inst.*, 2013, **34**, 279–287.
22 J. Badra, A. E. Elwardany, F. Khaled, S. S. Vasu and A. Farooq, *Combust. Flame*, 2014, **161**, 725−734.
23 D. F. Davidson, M. Roehrig and E. L. Petersen, *J. Quant. Spectrosc. Radiat. Transfer*, 1996, **55**, 755−762.
24 V.B. Oyeyemi, J.A. Keith and E.A. Carter, *J. Phys. Chem. A*, 2014, **118**, 7392–7403.
25 E. Wigner, Z. Phys. Chem. Abt. B, 1932, **19**, 203−216.
26 J. Wu, F. Khaled, H. Ning, L. Ma, A. Farooq and W. Ren, *J. Phys. Chem. A*, 2017, **121**, 6304–6313.
27 J.C. Lizardo-Huerta, B. Sirjean, R. Bounaceur and R. Fournet, *Phys. Chem. Chem. Phys.*, 2016, **18**, 12231−12251.
28 T. Seta, M. Nakajima and A. Miyoshi, *J. Phys. Chem. A*, 2006, **110**, 5081−5090.